INVESTIGATION ON CRACK NUCLEATION LOCATION IN FRETTING-AFFECTED AL 7050-T7451 ALLOY

Sabrina Vantadori[a], Andrea Zanichelli[a], Camilla Ronchei[b], Daniela Scorza[c], Andrea Carpinteri[a,*]

[a] Department of Engineering & Architecture, University of Parma, Parco Area delle Scienze 181/A, 43124 Parma, Italy

[b] Department of Civil Engineering, University of Calabria, via Pietro Bucci, 87036 Arcavacata di Rende (CS), Italy

[c] Department of Engineering, University of Naples Parthenope, Centro Direzionale Isola C4, 80143 Napoli, Italy

***Corresponding Author:** andrea.carpinteri@unipr.it

ABSTRACT

The present paper deals with the estimation of the crack nucleation orientation in fretting-affected Al 7050-T7451 specimens, subjected to cylindrical contact in partial slip regime. In such a context, cracks are generally assumed to nucleate at the contact trailing edge. However, experimental evidences of cracks starting within the contact zone are available in the literature. Therefore, a parametric study on the crack nucleation location is performed in the present work by using an analytical methodology. Four different crack nucleation locations

on the contact surface are examined, starting from the contact trailing edge and moving inside the micro-slip region.

KEYWORDS

Cylindrical contact, crack nucleation location, fretting partial slip, Ruiz parameter, 7050-T7451 Al alloy.

1. INTRODUCTION

Nowadays many in-service engineering components belonging to different application fields are still affected by catastrophic failures related to the fretting phenomenon **[1]**. Such failures generally occur in metallic structural components in contact to each other, experiencing vibrations or small relative oscillatory movements. In this case, high stress gradients and multiaxial stress state are expected near the contact zone **[2,3]**.

Fretting is a complex contact phenomenon which may be recognised in many different conditions, and involves more than 50 parameters **[4,5]**. Two different regimes can be identified depending on the relative micro-displacements field arising between the contact surfaces **[6]**:

- Gross slip regime, when global relative motion occurs between the structural components;
- Partial slip regime, when relative micro-displacements occur in the outer part (named slip region) of the contact surface, and no

relative motion occurs within the inner region (named stick region).

As is well-known, the main damage phenomenon related to fretting is the nucleation of cracks at the contact surface due to high stress gradients, which is typical of partial slip regime **[7,8]**. In more detail, micro-cracks may nucleate at the surface between the structural components in contact. Subsequently, such micro-cracks may propagate, leading to the fatigue failure of one of the components involved **[9]**.

Many efforts have been made in the past in order to understand the fretting damage process. It is now well-known that such a damage process is related to both geometry, loading, environmental conditions at macroscopic scale, and physical and chemical properties at the scale of the material microstructure **[10]**. Consequently, models related to both macroscopic approach and micromechanics approach have been proposed.

For instance, Endo and Goto **[11]** proposed to correlate the nucleation of inclined cracks with a combination of tangential stress and fully reversed bulk cyclic axial stress. Moreover, the principal stress directions computed at the crack nucleation site were used by Nishioka and Hirakawa **[12]** to determine the crack orientation. Subsequently, the principal stresses were employed by Nowell and Hills **[13]** together with the Mode I and Mode II Stress Intensity Factors, in order to evaluate cracks nucleating at the edge of the contact zone. A fatigue limit criterion related to both macroscopic and microscopic scales was proposed by

Dang Van et al. **[14]**. Although this criterion shows a good correlation with experimental results, a complex elastic-plastic stress-strain field computation including kinematic hardening is required.

It became thus clear that models strictly related to stress field were not adequate for predicting the fretting crack nucleation. In such a context, Nishioka and Hirakawa **[15]** associated the relative micro-slip amplitude with the nucleation and subsequent propagation of fretting cracks. Accordingly, Ruiz et al. **[16]** found a correlation between the crack nucleation location and both micro-slip amplitude and tensile and shear stresses parallel to the material surface. They obtained satisfactory estimations for three different materials, that is, a titanium alloy, a chromium alloy, and a nickel alloy. Subsequently, other researchers successfully employed the Ruiz parameter in order to determine the crack nucleation location **[17-20]**. However, the Ruiz parameter is not able to provide information related to crack path orientation or fatigue life of the structural component.

Recently, an analytical methodology **[21-24]** has been proposed by some of the present authors for fretting fatigue assessment of metallic structures. This methodology is based on the multiaxial fatigue criterion by Carpinteri et al. **[25-27]** and the Critical Direction Method (CDM) by Araujo et al. **[28,29]**, and incorporates a parameter related to the material microstructure (that is, the average material grain size). Several applications of such a

methodology are available in the literature, for different materials, fretting loading and contact configurations.

According to the original formulation of such a methodology **[21-24]**, the crack nucleation location is assumed to be at the edge of the contact, in quite good agreement with the experimental findings. In fact, in partial slip condition, the main cracks are expected to nucleate in correspondence of the stress concentration region, that is, at the edge of the contact. However, many cases of cracks nucleating within the contact zone (close to the contact edge) are available in the literature **[30,31]**.

Therefore, in the present research work the crack nucleation location is assumed to vary along the contact surface (within the micro-slip zone) in order to analyse the influence of such a location on fatigue assessment, in terms of both crack path orientation and lifetime.

To such an aim, an experimental campaign carried out on a 7050-T7451 aluminium alloy under cylindrical contact available in the literature **[32]** is examined.

A parametric study on the crack nucleation location (starting from the contact edge and moving inside the contact surface) is performed by employing the above analytical methodology. More precisely, different points within the micro-slip zone are alternatively assumed as crack nucleation location, and the methodology is applied for each of such locations.

The results obtained for each crack nucleation location are compared with the experimental crack path orientations as well as

with those determined by means of different methods available in the literature **[32]**.

Moreover, lifetime evaluations are compared with the experimental data.

The present paper is structured as follows. **Section 2** is devoted to outline the theoretical aspects on which the methodology is based, consisting in: the closed-form solution of the problem related to cylindrical contact in partial slip regime **[1,33-36]**, the multiaxial fatigue criterion by Carpinteri et al. **[25-27]**, and the Critical Direction Method **[28,29]**. Then, the analytical methodology employed for the simulation is presented in **Section 3**, whereas the experimental campaign carried out by Almeida et al. **[32]** is summarised in **Section 4**. The results obtained are reported and discussed in **Section 5**. Finally, conclusions are summarised in **Section 6**.

2. THEORETICAL ASPECTS

The theoretical aspects on which the analytical methodology is based are outlined here. More in detail, the analytical solution to determine both stress and strain fields in cylindrical contact problems subjected to fretting partial slip regime is firstly introduced **[1,33-36]**. Then, the main steps of the critical-plane based criterion, named Carpinteri et al. criterion **[25-27]**, originally proposed for the plain fatigue assessment of metallic structures under multiaxial constant amplitude cyclic loading, are

summarized. Finally, the Critical Direction Method (CDM) by Araujo et al. **[28,29]**, implemented in the methodology to determine the critical plane orientation, is described.

2.1 Closed-form solution for cylindrical contact in partial slip regime

The typical fretting testing configuration, where two cylindrical pads are clamped against a flat specimen in partial slip regime, is schematized in **Figure 1**. The reference frame $Oxyz$ is also shown in **Figure 1**, as well as a normal constant force P and a cyclic tangential force $Q(t)$, applied to the pads. The contact problem between the specimen and each of the two pads may be studied as a contact between two cylindrical bodies characterised by different radii of curvature, R_1 and R_2.

Figure 1.

First of all, let us consider the deformation (dotted line in **Figure 2 (a)**) endured by the cylindrical bodies, due to the application of a constant normal load P:

- two points T_1 and T_2 located inside of bodies 1 and 2, respectively, reasonably distant from the contact zone, move along the z-direction by an amount equal to δ_{z1} and δ_{z2}, respectively;

- two points S_1 and S_2 located (before deformation) on the surface of bodies 1 and 2, respectively, move along the z-direction by an amount equal to u_{z1} and u_{z2}, respectively.

Figure 2.

After the deformation, the contact zone is characterised by a width equal to $2a$. Under such a condition, it may result that points S_1 and S_2 are coincident, meaning that they are located within the contact region (that is, $-a \le x \le a$). In this case, the following equality holds **[33]**:

$$u_{z1} + u_{z2} = \delta_{z1} + \delta_{z2} - \frac{1}{2R} x^2 \qquad \textbf{(1)}$$

where R is the relative radius of curvature between the two bodies in contact:

$$\frac{1}{R} = \left(\frac{1}{R_1} + \frac{1}{R_2} \right) \qquad \textbf{(2)}$$

On the other hand, it may result that points S_1 and S_2 are not coincident, meaning that they are located outside the contact region (that is, $|x| > a$). In this case, the following inequality holds **[33]**:

$$u_{z1} + u_{z2} > \delta_{z1} + \delta_{z2} - \frac{1}{2R} x^2 \qquad \textbf{(3)}$$

Then, we can uniquely determine the normal pressure distribution, $p(x)$, that satisfies both Eq. (1) and Eq. (3) **[1,33]**, that is:

$$p(x) = \frac{2P}{\pi a^2}\sqrt{a^2 - x^2} \tag{4}$$

where the constant normal load P is given by:

$$P = \frac{\pi a^2 E^*}{4R} \tag{5}$$

and the semi-width of the contact zone a can be expressed as follows:

$$a = \sqrt{\frac{4PR}{\pi E^*}} \tag{6}$$

being E^* the elastic modulus for plane strain condition.

Such a distribution, named Hertzian pressure distribution, is characterized by a parabolic shape with a maximum value for $x=0$, given by:

$$p_0 = \frac{2P}{\pi a} \tag{7}$$

The components of the stress tensor in the vicinity of the contact zone, due to a constant normal load P, are given by **[34]**:

$$\sigma_x^P = -\frac{p_0}{a}\left[m\left(1 + \frac{z^2 + n^2}{m^2 + n^2}\right) - 2z \right] \tag{8a}$$

$$\sigma_z^P = -\frac{p_0}{a} m\left(1 - \frac{z^2 + n^2}{m^2 + n^2}\right) \tag{8b}$$

$$\tau_{xz}^P = \begin{cases} -\dfrac{p_0}{a} n\left(\dfrac{m^2 - z^2}{m^2 + n^2}\right) & \text{for } x \geq 0 \\ \dfrac{p_0}{a} n\left(\dfrac{m^2 - z^2}{m^2 + n^2}\right) & \text{for } x < 0 \end{cases} \tag{8c}$$

where m and n can be computed by the following expressions:

$$m^2 = \frac{1}{2}\left[\sqrt{\left(a^2 - x^2 + z^2\right)^2 + 4x^2 z^2} + \left(a^2 - x^2 + z^2\right) \right] \tag{9a}$$

$$n^2 = \frac{1}{2}\left[\sqrt{\left(a^2 - x^2 + z^2\right)^2 + 4x^2z^2} - \left(a^2 - x^2 + z^2\right)\right] \qquad \textbf{(9b)}$$

Now let us consider a constant tangential force Q, applied while maintaining constant the applied normal load P (see **Figure 2 (b)**).

If the above bodies in contact have the same elastic properties, the size and shape of the contact zone are not influenced by the presence of the tangential load.

On the other hand, in the case of two bodies in contact with different elastic properties, both the normal pressure distribution $p(x)$ and the size and shape of the contact zone are influenced by the presence of the tangential load. However, such an influence is negligible for small values of friction coefficient, which is typical of mechanical applications. Therefore, the effect of the normal load and that of the tangential load may be independently examined and, subsequently, both stress and deformation fields for the two conditions may be combined together according to the superposition principle.

The deformation of the cylindrical bodies, due to the application of the tangential load Q, is shown in **Figure 2 (b)**, where:

- the above two points T_1 and T_2 move along the x-direction by an amount equal to δ_{x1} and δ_{x2}, respectively;
- the two points A_1 and A_2 on the contact surfaces move along the x-direction by an amount equal to u_{x1} and u_{x2}, respectively.

After the deformation, the contact zone is characterised by an inner region (named stick region) where no relative displacements arise between the bodies, and an outer region (named slip region) where relative displacements arise between the bodies. The stick region is characterised by a width equal to $2c$. Under such a condition, the relative displacement in the x-direction between A_1 and A_2 (that is, the relative slip s_x between two points lying on the contact surface) may be expressed as follows:

$$s_x = \left(u_{x1} - \delta_{x1}\right) - \left(u_{x2} - \delta_{x2}\right) = \left(u_{x1} - u_{x2}\right) - \delta_x \qquad \textbf{(10)}$$

being $\delta_x = \delta_{x1} - \delta_{x2}$.

If points A_1 and A_2 are located within the stick region (that is, $-c \le x \le c$), s_x is equal to zero and no relative motion arises. Consequently, Eq. (10) becomes:

$$u_{x1} - u_{x2} = \delta_x \qquad \textbf{(11)}$$

On the other hand, if points A_1 and A_2 are located within the slip region (that is, $c < |x| \le a$), s_x is given by:

$$s_x = -\left(\frac{1-\nu_1^2}{E_1} + \frac{1-\nu_2^2}{E_2}\right)\frac{\mu p_0}{a}x^2 - \delta_x \qquad \textbf{(12)}$$

where ν_1, E_1 and ν_2, E_2 are the Poisson coefficient and the elastic modulus of the two bodies in contact, respectively. It is worth noticing that s_x is characterized by a parabolic shape: it is equal to zero for $|x| = c$ and increases by moving towards the contact edge (that is, $|x| = a$).

Moreover, in order to assure that no relative motion arises within the stick region (that is, $-c \le x \le c$), the contact shear distribution $q(x)$ must satisfy the following condition:

$$|q(x)| < \mu |p(x)| \tag{13}$$

being μ the friction coefficient between the two bodies in contact.

On the other hand, in order to assure that micro-slips arise within the slip region (that is, $c < |x| \le a$), the contact shear distribution $q(x)$ must satisfy the following condition:

$$|q(x)| = \mu |p(x)| \tag{14}$$

Then, it can be determined the contact shear distribution $q(x)$ that satisfies both Eqs. (11) and (13) within the stick region, and both Eqs. (12) and (14) within the slip region **[1,33,35,36]**:

$$q(x) = \begin{cases} \dfrac{\mu p_0}{a}\sqrt{a^2 - x^2} & \text{for } c \le |x| \le a \\ \dfrac{\mu p_0}{a}\left(\sqrt{a^2 - x^2} - \sqrt{c^2 - x^2}\right) & \text{for } |x| < c \end{cases} \tag{15}$$

where the semi-width c of the stick region is:

$$c = a\sqrt{1 - \frac{Q}{\mu P}} \tag{16}$$

The components of the stress tensor in the vicinity of the contact zone, due to a constant tangential load Q, are given by **[1]**:

$$\sigma_x^Q = \begin{cases} \dfrac{\mu p_0}{a}\left\{\left[n\left(2-\dfrac{z^2-m^2}{m^2+n^2}\right)-2x\right]-\left[n_c\left(2-\dfrac{z^2-m_c^2}{m_c^2+n_c^2}\right)-2x\right]\right\} \\ \text{for } x \geq 0 \\ \dfrac{\mu p_0}{a}\left\{-\left[n\left(2-\dfrac{z^2-m^2}{m^2+n^2}\right)+2x\right]+\left[n_c\left(2-\dfrac{z^2-m_c^2}{m_c^2+n_c^2}\right)+2x\right]\right\} \\ \text{for } x < 0 \end{cases} \quad \textbf{(17a)}$$

$$\sigma_z^Q = \begin{cases} \dfrac{\mu\, p_0}{a}\left[-n\left(\dfrac{m^2-z^2}{m^2+n^2}\right)+n_c\left(\dfrac{m_c^2-z^2}{m_c^2+n_c^2}\right)\right] & \text{for } x \geq 0 \\ \dfrac{\mu\, p_0}{a}\left[n\left(\dfrac{m^2-z^2}{m^2+n^2}\right)-n_c\left(\dfrac{m_c^2-z^2}{m_c^2+n_c^2}\right)\right] & \text{for } x < 0 \end{cases} \quad \textbf{(17b)}$$

$$\tau_{xz}^Q = \frac{\mu\, p_0}{a}\left\{-\left[m\left(1+\frac{z^2+n^2}{m^2+n^2}\right)-2z\right]+\left[m_c\left(1+\frac{z^2+n_c^2}{m_c^2+n_c^2}\right)-2z\right]\right\} \quad \textbf{(17c)}$$

where m_c and n_c can be computed by the following expressions:

$$m_c^2 = \frac{1}{2}\left[\sqrt{\left(c^2-x^2+z^2\right)^2+4x^2z^2}+\left(c^2-x^2+z^2\right)\right] \quad \textbf{(18a)}$$

$$n_c^2 = \frac{1}{2}\left[\sqrt{\left(c^2-x^2+z^2\right)^2+4x^2z^2}-\left(c^2-x^2+z^2\right)\right] \quad \textbf{(18b)}$$

2.2 The Carpinteri et al. criterion

The main steps of the critical-plane based criterion, named Carpinteri et al. criterion **[25-27]**, originally proposed for the plain fatigue assessment of metallic structures under multiaxial constant amplitude cyclic loading, are hereafter summarized.

According to the above criterion, the fatigue assessment of a structural component consists of two steps: the first one deals with the determination of the critical plane orientation, whereas the second one deals with the fatigue life evaluation carried out in such a plane. In more details, the fatigue life evaluation is

performed by employing an equivalent stress amplitude computed after the reduction of the multiaxial stress state to an equivalent uniaxial one.

Let us consider the stress tensor $\boldsymbol{\sigma}(t)$ in a generic point of a metallic body under cyclic loading. Both principal stresses $\sigma_1,\sigma_2,\sigma_3$ (with $\sigma_1>\sigma_2>\sigma_3$) and the corresponding principal directions $1,2,3$ in such a point are generally time-varying. According to the Carpinteri et al. criterion, the averaged values of the principal stresses within a loading cycle can be identified, which are those corresponding to the time instant when σ_1 attains its maximum value within a loading cycle. Then, the averaged principal stress directions can be also determined. Finally, the orientation of the critical plane is identified assuming the normal to such a plane to be rotated with respect to the averaged maximum principal stress direction by an angle which is a function of the material fatigue strengths $\sigma_{af,-1}$ and $\tau_{af,-1}$ under fully reversed normal and shear loading, respectively (related to a reference number N_0 of loading cycles).

Once the orientation of the critical plane has been determined, the stress components acting on such a plane are computed. The normal stress component perpendicular to the critical plane is characterized by a fixed direction with respect to time and, consequently, both the mean value N_m and the amplitude N_a are easily determined. On the other hand, since the shear stress component lying on the critical plane has a time-

varying direction, the amplitude C_a is uniquely computed by means of the Maximum Rectangular Hull method **[37]**.

Finally, the number of loading cycles to failure, $N_{f,cal}$, may be determined by iteratively solving the following equation:

$$\sqrt{N_{eq,a}{}^2 + \left(\frac{\sigma'_{af,-1}}{\tau'_{af,-1}}\right)^2 C_a^2} = \sigma'_{af,-1} \qquad \textbf{(19)}$$

where $N_{eq,a}$ is the amplitude of the equivalent normal stress acting on the critical plane, given by the like-Goodman equation **[38]**:

$$N_{eq,a} = N_a + \sigma_{af,-1}\left(\frac{N_m}{\sigma_u}\right) \qquad \textbf{(20)}$$

and $\sigma'_{af,-1}$ and $\tau'_{af,-1}$ are the finite life fatigue strengths proposed by Basquin **[39]** for the finite fatigue life evaluation:

$$\sigma'_{af,-1} = \sigma_{af,-1}\left(\frac{N_{f,cal}}{N_0}\right)^m \qquad \textbf{(21a)}$$

$$\tau'_{af,-1} = \tau_{af,-1}\left(\frac{N_{f,cal}}{N_0}\right)^{m*} \qquad \textbf{(21b)}$$

being σ_u the ultimate tensile strength, and m and $m*$ the slopes of the S-N curves under fully reversed normal and shear loading, respectively.

2.3 The Critical Direction Method

The Critical Direction Method (CDM) proposed by Araujo et al. **[28,29]** is herein employed to determine the critical plane.

In a fretting testing configuration, the problem is typically two-dimensional, and therefore the critical plane is represented

by a segment, with a given length l, starting from the hot-spot. The segment orientation α is defined by the angle between the segment and the line perpendicular to the surface of the structural component, starting from the hot-spot. Positive values of α are considered when the segment is towards the centre of the contact zone.

According to the CDM, a fatigue parameter is computed along each of the segments obtained by varying α in the range $-90° \le \alpha \le +90°$, with an angular increment equal to $\Delta\alpha$, that is, assuming each segment as a candidate to be the critical plane. The above fatigue parameter is a function of stress quantities, averaged along the segment. The orientation of the critical plane, α_{cr}, is determined by maximising such a parameter.

3. ANALITICAL METHODOLOGY FOR FRETTING ASSESSMENT

This Section is devoted to the description of the methodology, proposed by some of the present authors, to perform the fretting assessment of metallic structures subjected to cylindrical contact in partial slip regime **[21-24]**. The algorithm of such a methodology is shown in **Figure 3**.

Figure 3.

The *input data* are represented by the geometric sizes (that is, pad radius R, thickness B, and width W of the specimen) and

the loading conditions (normal load P, tangential load Q, and bulk stress σ_B) of the contact problem, the material properties (elastic modulus E, Poisson coefficient ν, ultimate tensile strength σ_u, friction coefficient μ, average grain size d) and the fatigue properties (material fatigue strengths $\sigma_{af,-1}$ and $\tau_{af,-1}$, and slope of the S-N curve m and m^*, under fully reversed normal and shear loading, respectively, at a reference number N_0 of loading cycles) of the structural component to be analysed.

Firstly, the *stress state* within the component is computed by employing the analytical solution described in Section 2.1 (see the algorithm block in red in **Figure 3**).

Then, the *crack nucleation location* (also named hot-spot in the following) on the material surface needs to be defined.

Successively, the orientation of the critical plane, α_{cr}, is determined according to the *Critical Direction Method* (CDM) described in Section 2.3 (see the algorithm block in grey in **Figure 3**). The physical size l associated to the critical plane is here assumed to be equal to twice the average grain size of the material, $2d$. The fatigue parameter here employed, $N_{eq,a}(\alpha)$, is computed according to Eq. (20), where N_a and N_m are replaced by their averaged values, computed along each $\alpha-$oriented segment.

Finally, the fatigue lifetime $N_{f,cal}$ is determined according to the *Carpinteri et al. criterion* **[25-27]** (described in Section 2.2), highlighted in **Figure 3** (see the algorithm block in blue).

More precisely, $N_{f,cal}$ is computed through Eq. (19), by employing the stress components acting on the critical plane at the verification point S_{cr} located at the end of the abovementioned segment, that is, $N_a(2d,\alpha_{cr})$, $N_m(2d,\alpha_{cr})$, and $C_a(2d,\alpha_{cr})$.

4. EXPERIMENTAL CAMPAIGN ANALYSED

In the present paper, the experimental campaign carried out by Almeida et al. **[32]** at the University of Brasilia is analysed. More in detail, fretting tests in partial slip regime were performed by employing a fretting machine with two independent hydraulic actuators. The cylindrical pads were pushed against a flat dog-bone specimen with a square cross section of 13x13 mm. Two different values of pad radius were considered, that is, 30 mm and 70 mm.

Both specimens and pads were made of 7050-T7451 aluminium alloy. The chemical composition **[32]** is reported in **Table 1**, whereas the mechanical **[32]** and fatigue **[40]** properties are listed in **Table 2**. This aluminium alloy is characterized by an average size d of the small grains equal to 8 microns and a friction coefficient μ equal to 0.54 **[41]**.

Table 1.

Table 2.

Eight different fretting loading configurations were examined, and a total of 19 specimens were tested. When present, a constant

bulk load σ_B was first applied to the specimen in order to avoid the off-set of the stick zones during the test. Subsequently, after the pads were pushed against the specimen by means of a constant normal load P, a cyclic tangential load $Q(t)$ was applied to the pads, with a loading ratio equal to -1 and a frequency equal to 10 Hz.

For pad radius $R = 70mm$ (test Nos T1, T2, T3, T7, and T8), three different values of tangential load amplitude were considered. Moreover, for the medium level of tangential load amplitude, three different values of bulk load were examined. For $R = 30mm$ (test Nos T4, T5, and T6), a single value of tangential load amplitude was considered, and three different values of bulk load were examined.

The values of constant normal load, amplitude of the tangential load and constant bulk load are listed in **Table 3** for each loading configuration, together with the theoretical semi-widths of both the contact zone a (see Eq. (6)) and the stick zone c (see Eq. (16)).

All the tests were stopped at 10^6 loading cycles in order to analyse the experimental crack paths. The fretting loading conditions were designed so that the expected number of loading cycles to failure was slightly higher than 10^6 and, consequently, the crack paths were clearly evident. Note that one specimen of the test configuration T8 failed at $9.2 \cdot (10)^5$ loading cycles.

Each specimen was transversely cut after testing in correspondence of the symmetry plane, and subsequently covered by

means of a phenolic resin. Then, they were sanded, polished, chemically treated with a Keller's solution for 12 seconds, washed in tap water and, finally, analysed by employing a confocal microscope.

The cracks were generally observed to nucleate within the contact zone, close to the contact trailing edge. In particular, cracks were found within the slip zone, in a region between the contact trailing edge and the centre of the slip zone (that is, $(c+a)/2 \leq x \leq a$). Such cracks were characterised by an orientation α_{exp} (defined from the line perpendicular to the surface of the component, with positive values if the crack is towards the centre of the contact zone) ranging from 7° to 56°. The crack path orientations observed during the experimental campaign are listed in **Table 4** for each loading configuration tested. Note that such angles were measured at a depth equal to 56.5 microns.

Table 4.

5. RESULTS AND DISCUSSION

The experimental campaign, available in the literature **[32]** and described in Section 4, is here analysed through the analytical methodology recently proposed by some of the present Authors **[21-24]** and summarized in Section 3, where the crack nucleation location is assumed to vary along the contact surface (within the micro-slip zone) in order to analyse its influence on the fatigue assessment in terms of both crack path orientation and lifetime.

The physical size l of the critical plane is assumed to be equal to $2d$=16μm, and the angular increment $\Delta\alpha$ is set equal to $1°$.

Four different hot-spots (that is, $i_{max}=4$) on the contact surface are examined, that is (**Figure 4**):

- point A: characterised by the maximum value of the maximum principal stress expected within a fretting cycle, and located at the trailing edge of the contact (that is, $x=a$). As a matter of fact, according to the original formulation of the present methodology, the hot-spot is assumed to be the above point. This outcome is in general in agreement with the expectation that the main cracks should nucleate in correspondence of the stress concentration region, that is, at the edge of the contact for cylindrical fretting problems in partial slip regime;
- point B: characterised by the maximum value of the Ruiz parameter k expected within a fretting cycle, and generally located within the slip zone close to the trailing edge of the contact (that is, $c<x\leq a$). As a matter of fact, during the experimental campaign reported in Section 4 **[32]**, cracks were found to nucleate within the contact zone close to the trailing edge. Therefore, the point on the material surface, where the maximum value of the Ruiz parameter k **[16]** within a fretting cycle is attained, is here taken as the hot-spot, being:

$$k=\sigma_x\tau_{xz}s_x \qquad \textbf{(22)}$$

where σ_x and τ_{xz} are the normal and shear stresses acting parallel to the material surface, and s_x is the amplitude of the relative micro-slip between the bodies in contact (see Section 2);

- point C: located in the centre of the slip zone (that is, $x=(c+a)/2$);
- point D: located at the boundary between the slip zone and the stick zone (that is, $x=c$).

Figure 4.

It is worth noticing that points C and D are not related to the stress field within the component, and are not related to the relative slip conditions at the contact interface. On the other hand, point A is related to the stress field within the component, A being the point where the maximum value of the maximum principal stress is expected within a loading cycle, but it does not take into account the relative slip conditions at the contact interface. Moreover, point B is related to both the stress field within the component, and the relative slip conditions at the contact interface (see Eq. (22)).

The algorithm blocks named Critical Direction Method and Carpinteri et al. criterion in **Figure 3** are passed for each hot-spot location examined, that is, for four times being $i_{max}=4$.

The results determined by taking into account the above four crack nucleation locations are graphically reported in **Figure 5** for each test configuration examined.

Figure 5.

The values of crack path orientation evaluated are listed in **Table 4.** It can be noted that all the orientations obtained are towards the centre of the contact region, in accordance to the experimental observations. Moreover, as the crack nucleation location moves inward the contact region (that is, from point A to point D), the estimated values of crack orientation increase, with values between 4° and 5° at point A, between 16° and 18° at point B, between 24° and 27° at point C, and between 43° and 48° at point D.

The accuracy of such evaluations may be quantified by employing the root mean square error method **[42,43]**, being the value of the root mean square error given by:

$$T_{RMS} = 10^{\sqrt{\frac{\sum_{j=1}^{19} Log^2\left(\alpha_{th,i}/\alpha_{exp}\right)_j}{19}}} \qquad i = 1,...4 \tag{23}$$

The values of T_{RMS} for crack orientation estimations related to points A, B, C and D are equal to 1.632, 1.437, 1.313 and 1.309 (see **Figure 6**), respectively, thus highlighting that better estimations in terms of crack path orientations are determined by considering the hot-spot within the contact zone (points B, C and D) instead of at the edge of the contact (point A). As a matter of fact, a value of root mean square error equal to 1 would correspond to a perfect correlation between theoretical estimations and experimental evidences.

Figure 6.

The number of loading cycles to failure, $N_{f,cal}$, evaluated by assuming points A, B, C, and D as crack nucleation locations, is shown in **Figure 7** for each test configuration examined.

Figure 7.

As the crack nucleation location moves inward the contact region (that is, from point A to point D), the estimated values of $N_{f,cal}$ increase. Moreover, it can be noted that the results related to both points A and B seem to be more accurate than those related to both points C and D, and more precisely:

- when point A is assumed as the hot-spot, the values obtained are slightly lower or slightly higher than the experimental run-out limit;

- when point B is assumed as the hot-spot, the values obtained are slightly higher than the experimental run-out limit;

- when either point C or point D are assumed as hot-spot, the values obtained are significantly higher than the experimental run-out limit.

Further, it may be interesting to compare the above results in terms of crack path orientations with those obtained by considering the crack nucleation location in correspondence of the contact trailing edge, and by employing three different fatigue parameters: Fatemi and Socie (FS) parameter, Modified Wohler Curve Method (MWCM) parameter, and Smith Watson and Topper (SWT)

parameter **[32].** The crack nucleation directions estimated were outward the contact region by employing the Fatemi and Socie parameter whereas, when either the Modified Wohler Curve Method parameter or the Smith Watson and Topper parameter were used, estimated cracks inward the contact region or almost perpendicular to the contact surface were obtained, respectively. The values of T_{RMS} for the crack orientations evaluated by employing either the FS, or the MWCM, or the SWT parameter, are equal to 2.319, 2.617, and 1.678, respectively **[32]** (see **Figure 8**).

Figure 8.

6. CONCLUSIONS

In the present paper, the crack path orientations of a 7050-T7451 aluminium alloy subjected to constant amplitude fretting loading have been examined by means of an analytical methodology recently proposed by some of the present authors. Such a methodology is based on both the multiaxial fatigue criterion by Carpinteri et al. and the Critical Direction Method (CDM) by Araujo et al., and incorporates a parameter related to the material microstructure (that is, the average material grain size).

An experimental campaign available in the literature, related to Al 7050-T7451 fretting-affected specimens subjected to cylindrical contact in partial slip regime, has been simulated by employing the above methodology. Since cracks have been

experimentally observed to occur within the contact zone close but not coincident with the trailing edge, a parametric study on the crack nucleation location has been performed in the present research work to evaluate the influence of such a location on the crack path orientation and lifetime. More precisely, four different crack nucleation locations on the contact surface have been examined, starting from the contact trailing edge and moving inside the contact surface, in the region where relative micro-slips arise.

As far as the estimated crack path orientations are concerned, the best results (that is, the lower value of T_{RMS}) have been obtained when the point D, located at the boundary between the slip zone and the stick zone, has been used as the hot-spot. However, for such a point, the lifetime values obtained are significantly higher than the experimental run-out limit.

As far as both the estimated crack path orientations and the lifetime are concerned, the results obtained when the point B, characterised by the maximum value of the Ruiz parameter within a fretting cycle, is assumed as the hot-spot are the most consistent with the experimental findings. Therefore, such a point has proved to be a good candidate as the crack nucleation location.

In conclusion, a high level of accuracy has been achieved by means of the analytical methodology employed, in terms of both crack path orientations and fatigue life. It can be noticed that the present estimations are more consistent with the experimental

findings than those determined by Almeida and co-workers employing different fatigue parameters.

Acknowledgements

The work of Sabrina Vantadori, Andrea Zanichelli and Andrea Carpinteri is supported by Italian Ministry of University and Research (P.R.I.N. National Grant 2017, Project code 2017HFPKZY; University of Parma Research Unit).

REFERENCES

[1] Johnson K.L. Contact Mechanics. UK: Cambridge University Press; 1985.

[2] Said J., Fouvry S., Cailletaud G., Yang C., Hafid F., Shear driven crack arrest investigation under compressive state: Prediction of fretting fatigue failure of aluminium strands, International Journal of Fatigue, 2020; 136: 105589.

[3] Vantadori S., Vázquez J., Zanichelli A., Fretting fatigue and shot peening: a multiaxial fatigue criterion including residual stress relaxation, Tribology International, 2020; 151: 106537.

[4] Collins J.A., Fretting-fatigue damage-factor determination, Journal of Engineering for Industry, 1965; 87, 3: 298-302.

[5] Pinto A.L., Talemi R., Araújo J.A., Fretting fatigue total life assessment including wear and a varying critical distance, International Journal of Fatigue, 2022; 156: 106589.

[6] Waterhouse R.B., Fretting fatigue, International Materials Reviews, 1992; 37: 77-97.

[7] Waterhouse R.B., Lindley T., 1994. Fretting Fatigue. London, UK, ESIS Publications.

[8] Carpinteri A., Vantadori S., Zanichelli A., Lifetime estimation of mechanical assemblies under constant amplitude fretting fatigue loading, Fatigue and Fracture of Engineering Materials and Structures, 2019; 42: 1927-1936.

[9] Vantadori S., Abbasi F., Zanichelli A., Leonetti D., Pucillo G.P., Majzoobi G.H., Influence of normal load frequency on fretting fatigue behaviour by a critical plane-based approach, International Journal of Fatigue, 2022: In press.

[10] Szolwinski M.P., Farris T.N., Mechanics of fretting fatigue crack formation, Wear, 1996; 198: 93-107.

[11] Endo K., Goto H., Initiation and propagation of fretting fatigue cracks, Wear, 1988; 125: 129-146.

[12] Nishioka K., Hirakawa K., Fundamental investigations of fretting fatigue, part 3, Bulletin of JSME, 1969; 12, 51: 397-407.

[13] Nowell D., Hills D.A., Mechanics of fretting fatigue tests, International Journal of Mechanical Sciences, 1987; 29: 355-365.

[14] Dang Van K., Griveau B., Message O., 1985. On a new multiaxial fatigue limit criterion: Theory and application. in Biaxial and Multiaxial Fatigue, ASTM, Philadelphia, 479-496.

[15] Nishioka K., Hirakawa K., Fundamental investigations of fretting fatigue, part 2, Bulletin of JSME, 1969; 12, 50: 180-187.

[16] Ruiz C., Boddington P.H.B., Chen K.C., An investigation of fatigue and fretting in a dovetail joint, Experimental Mechanics, 1984; 24, 3: 208-217.

[17] Kuno M., Waterhouse R.B., Nowell D., Hills D.A., Initiation and growth of fretting fatigue cracks in the partial slip regime, Fatigue & Fracture of Engineering Materials & Structures, 1989; 12, 5: 387-398.

[18] Bhatti N.A., Wahab M.A., Finite element analysis of fretting fatigue under out of phase loading conditions, Tribology International, 2017; 109: 552–562.

[19] Deng Q., Yin X., Wahab M.A., The Effect of Surface Pit Treatment on Fretting Fatigue Crack Initiation, Computers, Materials & Continua, 2021; 66, 1: 659-673.

[20] Sunde S.L., Haugen B., Berto F., Experimental and numerical fretting fatigue using a new test fixture, International Journal of Fatigue, 2021; 143: 106011.

[21] Vantadori S., Zanichelli A., Araújo J.A., Fretting fatigue of 7050-T7451 Al alloy: the influence of bulk mean stress, International Journal of Fatigue, 2020; 140: 105816.

[22] Vantadori S., Vázquez J., Zanichelli A., Carpinteri A., Luciano R., Structural integrity of shot peened Ti6Al4V specimens under fretting fatigue, International Journal of Fracture, 2021.

[23] Vantadori S., Zanichelli A., Fretting-fatigue analysis of shot-peened aluminium and titanium test specimens, Fatigue & Fracture of Engineering Materials & Structures, 2021; 44, 2: 397-409.

[24] Zanichelli A., Vantadori S., Shot-peened fretting fatigue components: Endurance strength and fatigue life assessment, Material Design and Processing Communications, 2021; 3, 4: e196.
[25] Carpinteri A., Ronchei C., Scorza D., Vantadori S., Critical plane orientation influence on multiaxial high-cycle fatigue assessment, Physical Mesomechanics, 2015; 18, 4: 348-354.
[26] Vantadori S., Carpinteri A., Luciano R., Ronchei C., Scorza D., Zanichelli A., Okamoto Y., Saito S., Itoh T., Crack initiation and life estimation for 316 and 430 stainless steel specimens by means of a critical plane approach, International Journal of Fatigue, 2020; 138: 105677.
[27] Vantadori S., Ronchei C., Scorza D., Zanichelli A., Carpinteri A., Fatigue behaviour assessment of ductile cast iron smooth specimens, International Journal of Fatigue, 2021; 152: 106459.
[28] Araújo J.A., Almeida G.M.J., Ferreira J.L.A., da Silva C.R.M., Castro F.C., Early cracking orientation under high stress gradients: the fretting, International Journal of Fatigue, 2017; 100: 302-311.
[29] Araújo J.A., Castro F.C., Matos I.M., Cardoso R.A., Life prediction in multiaxial high cycle fretting fatigue, International Journal of Fatigue 2020; 134: 105504.
[30] Venkatesh T.A., Conner B.P., Suresh S., Giannakopoulos A.E., Lindley T.C., Lee C.S., An experimental investigation of fretting fatigue in Ti-6Al-4V: The role of contact conditions and microstructure, Metallurgical and Materials Transactions A: Physical Metallurgy and Materials Science, 2001; 32, 5, 124: 1131-1146.
[31] Vázquez J., Navarro C., Domínguez J., Analysis of fretting fatigue initial crack path in Al7075-T651 using cylindrical contact, Tribology International, 2017; 108: 87-94.
[32] Almeida G.M.J., Pessoa G.C.V., Cardoso R.A., Castro F.C., Araújo J.A., Investigation of crack initiation path in AA7050-T7451 under fretting conditions, Tribology International, 2020; 144: 106103.

[33] Hertz H. Miscellaneous Paper by Heinrich Hertz. New York: Macmillan & Co; 1896.

[34] McEwen E., Stress in elastic cylinders in contact along a generatrix, Philosophical Magazine, 1949; 40: 454.

[35] Cattaneo C., Sul contatto di due corpi elastici: distribuzione locale degli sforzi, Rendiconti dell'Accademia Nazionale dei Lincei, 1938; 27, 6: 342–8.

[36] Mindlin R.D., Compliance of elastic bodies in contact, ASME Journal of Applied Mechanics, 1949; 16: 259–68.

[37] Araújo J.A., Carpinteri A., Ronchei C., Spagnoli A., Vantadori S., An alternative definition of the shear stress amplitude based on the Maximum Rectangular Hull method and application to the C-S (Carpinteri-Spagnoli) criterion. Fatigue & Fracture of Engineering Materials & Structures, 2014; 37: 764-771.

[38] Goodman J. Mechanics Applied to Engineering. Longmans Green, London; 1899.

[39] Basquin O.H., The exponential law of endurance tests, Proceedings of the American Society for Testing and Materials, 1910; 10: 625-630.

[40] Chen H., Shang D.-G., Tian Y.-J., Liu J.-Z., Comparison of multiaxial fatigue damage models under variable amplitude loading, Journal of Mechanical Science and Technology, 2012; 26: 3439-3446.

[41] Rossino L.S., Castro F.C., Bose Filho W.W., Araújo J.A., Issues on the mean stress effect in fretting fatigue of a 7050-T7451 Al alloy posed by new experimental data, International Journal of Fatigue, 2009; 31: 2041-2048.

[42] Vantadori S., Carpinteri A., Luciano R., Ronchei C., Scorza D., Zanichelli A., Mean stress effect on fatigue life estimation for Inconel 718 alloy, International Journal of Fatigue, 2020; 133: 105391.

[43] Vantadori S., Ronchei C., Scorza D., Zanichelli A., Araújo L.C., Araújo J.A., Influence of non-metallic inclusions on the high cycle fatigue strength of steels, International Journal of Fatigue, 2022; 154: 106553.

NOMENCLATURE

a	theoretical Hertzian contact half-width
d	average grain size
E	Young modulus
m	slope of the S-N curve under fully reversed normal loading
m^*	slope of the S-N curve under fully reversed shear loading
N_a	amplitude of the normal stress acting on the critical plane
N_m	mean value of the normal stress acting on the critical plane
$N_{eq,a}$	equivalent normal stress amplitude
$\bar{N}_a$	averaged value of N_a
$\bar{N}_m$	averaged value of N_m
P	normal force applied to the pads
Q	tangential load applied to the pads
Q_a	amplitude of the cyclic tangential load
R	pad radius
t	time

α_{cr}	orientation of the critical plane
α_{exp}	crack path orientation experimentally observed
α_{th}	crack path orientation theoretically estimated
μ	friction coefficient
ν	Poisson ratio
$\sigma_{af,-1}$	material fatigue strength under fully reversed normal loading, at a reference number N_0 of loading cycles
σ_B	axial bulk stress applied to the specimen
σ_u	ultimate tensile strength
$\sigma_1, \sigma_2, \sigma_3$	principal stresses
$\tau_{af,-1}$	material fatigue strength under fully reversed shear loading, at a reference number N_0 of loading cycles

INVESTIGATION ON CRACK NUCLEATION LOCATION IN FRETTING-AFFECTED AL 7050-T7451 ALLOY

Sabrina Vantadori[a], Andrea Zanichelli[a], Camilla Ronchei[b], Daniela Scorza[c], Andrea Carpinteri[a,*]

[a] Department of Engineering & Architecture, University of Parma, Parco Area delle Scienze 181/A, 43124 Parma, Italy

[b] Department of Civil Engineering, University of Calabria, via Pietro Bucci, 87036 Arcavacata di Rende (CS), Italy

[c] Department of Engineering, University of Naples Parthenope, Centro Direzionale Isola C4, 80143 Napoli, Italy

***Corresponding Author:** andrea.carpinteri@unipr.it

FIGURES AND TABLES

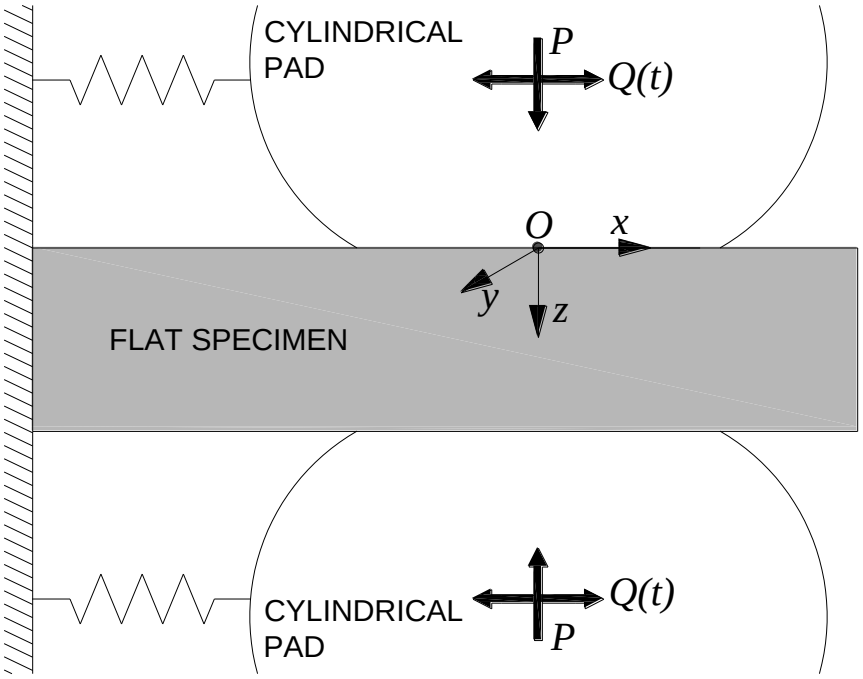

Figure 1. Typical cylinder-to-flat fretting fatigue test, under both constant normal force P and cyclic tangential force $Q(t)$.

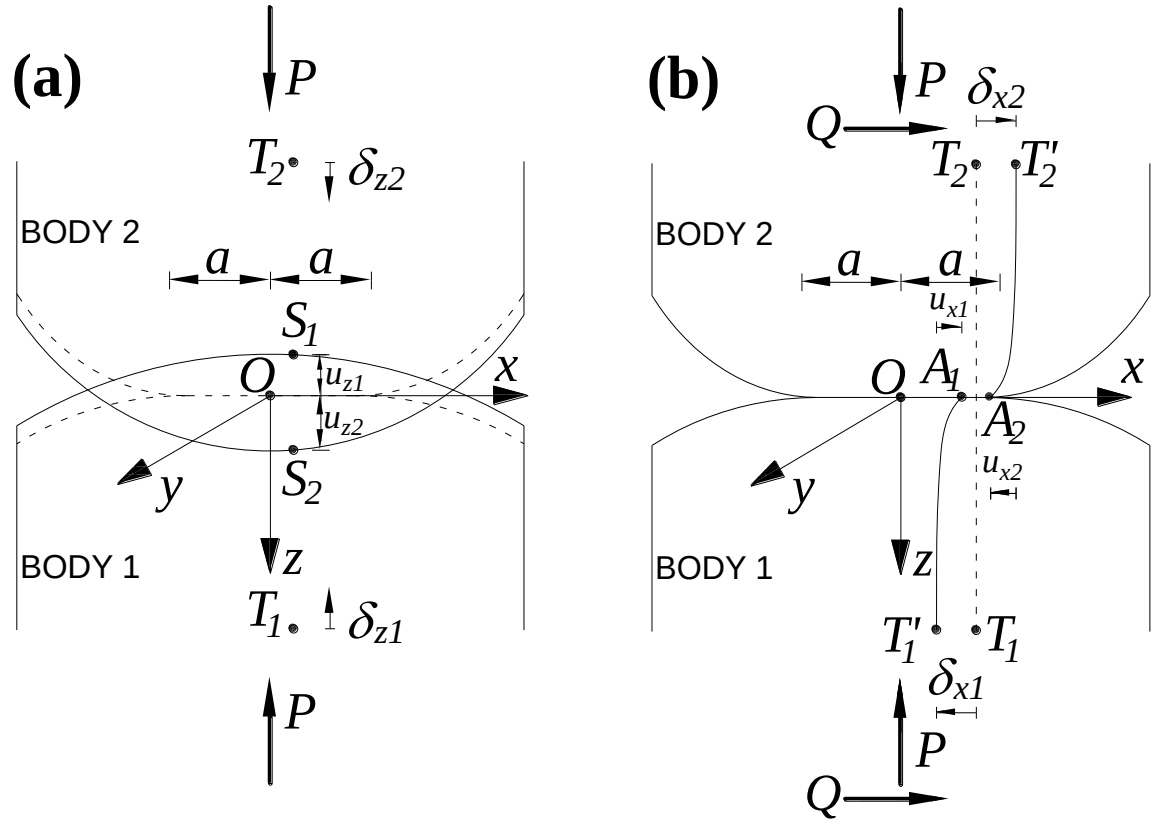

Figure 2. Cylindrical bodies in contact: (a) deformation due to a constant normal load P (dashed lines); (b) deformation due to a constant tangential load Q in addition to the normal load.

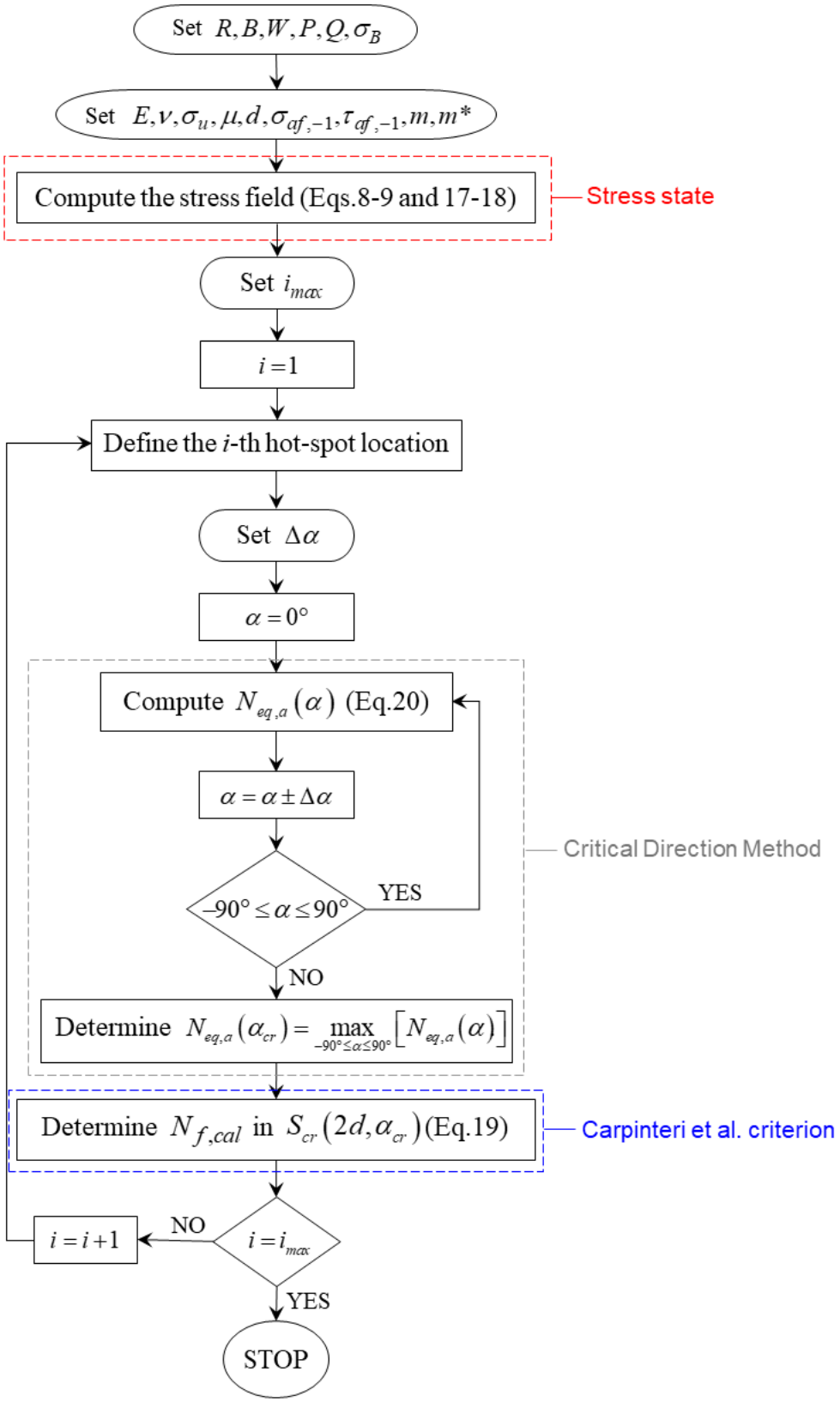

Figure 3. Algorithm of the analytical methodology employed.

Table 1. Chemical composition of 7050-T7451 aluminium alloy (in percentage by weight) **[32].**

MATERIAL	Zn	Mg	Cu	Fe	Zr	Si	Mn	Ti	Cr
Al 7050-T7451	6.2	2.3	2.3	0.15	0.13	0.12	0.09	0.06	0.006

Table 2. Mechanical and fatigue properties of 7050-T7451 aluminium alloy **[32,40].**

MATERIAL	E [GPa]	ν [-]	σ_u [MPa]	$\sigma_{af,-1}$ [MPa]	m [-]	$\tau_{af,-1}$ [MPa]	m^* [-]	N_0 [cycles]
Ref.	**[32]**	**[32]**	**[32]**	**[40]**	**[40]**	**[40]**	**[40]**	**[40]**
Al 7050-T7451	71.7	0.33	524	301	-0.05	127	-0.08	$2 \cdot 10^6$

Table 3. Fretting loading conditions for each test examined **[32].**

TEST No.	R [mm]	P [N]	Q_a [N]	σ_B [MPa]	a [mm]	c [mm]
T1	70	800	240	0	1.34	0.89
T2	70	800	320	0	1.34	0.68
T3	70	800	400	0	1.34	0.36
T4	30	341	136	0	0.57	0.29
T5	30	341	136	25	0.57	0.29
T6	30	341	136	50	0.57	0.29
T7	70	800	320	25	1.34	0.68
T8	70	800	320	50	1.34	0.68

Table 4. Crack path orientation experimentally observed **[32]** and estimated with either A, B, C, or D as the crack nucleation location, for each test examined.

Test No.	α_{exp} [°]	$\alpha_{th,A}$ [°]	$\alpha_{th,B}$ [°]	$\alpha_{th,C}$ [°]	$\alpha_{th,D}$ [°]
T1	7.3-41.5	5.0	18.0	24.0	43.0
T2	24.8-37.5	5.0	17.0	25.0	43.0
T3	32.5-37.0	4.0	16.0	27.0	44.0
T4	24.2-39.9	7.0	17.0	25.0	43.0
T5	31.3-31.7	7.0	17.0	25.0	45.0
T6	33.7-36.3	7.0	17.0	25.0	48.0
T7	17.3-54.4	5.0	17.0	25.0	46.0
T8	32.8-55.6	5.0	17.0	25.0	48.0

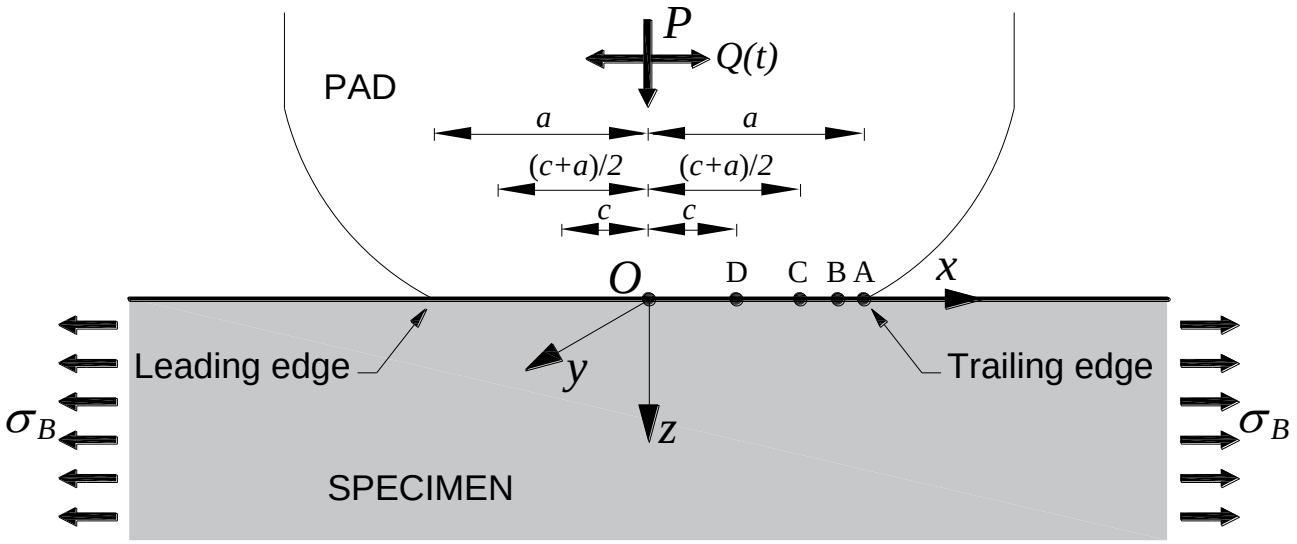

Figure 4. Different crack nucleation locations considered on the contact surface.

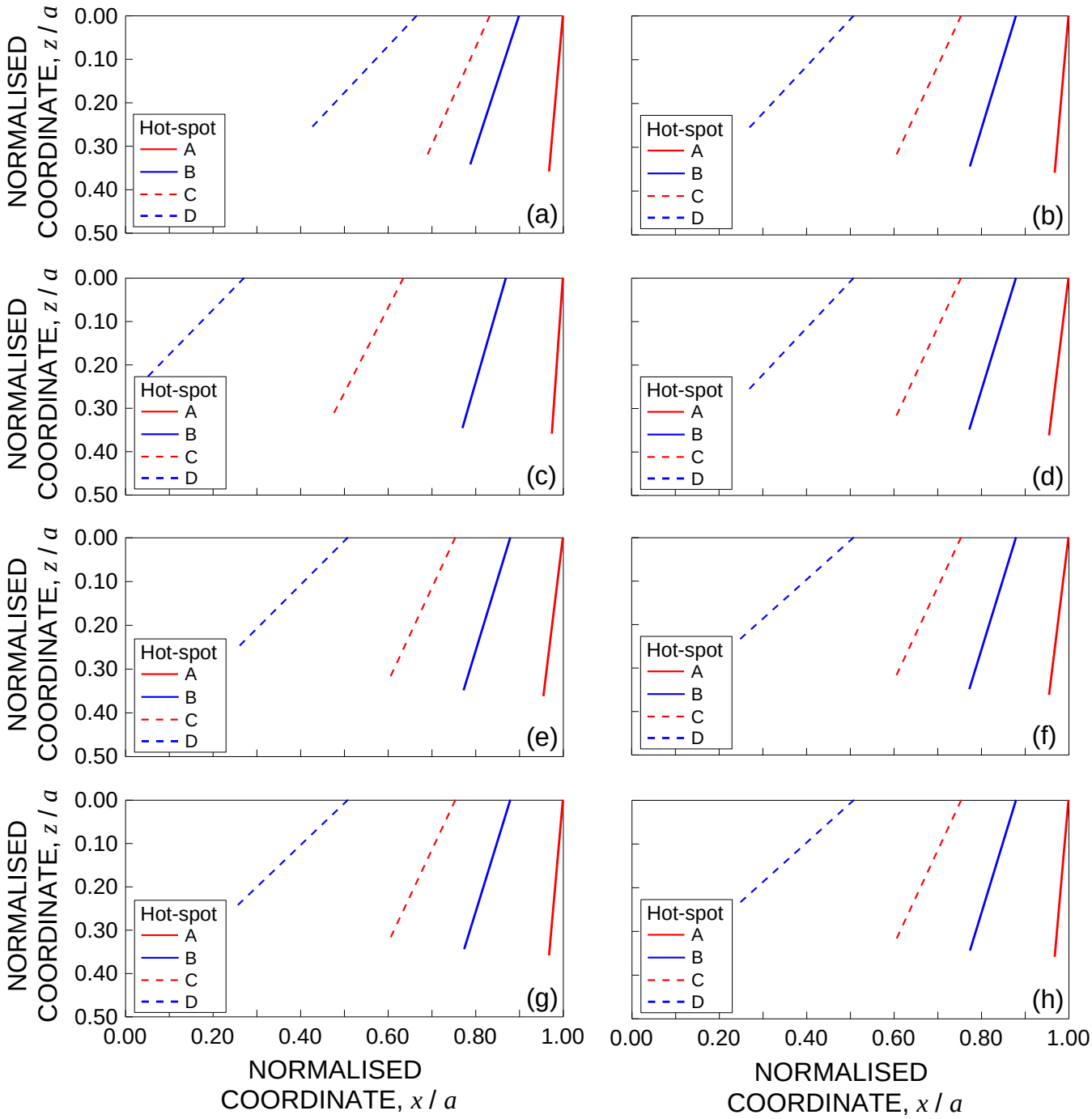

Figure 5. Crack path orientation evaluated by varying the hot-spot location (that is, point A, B, C, or D) for test configuration No.: (a) T1, (b) T2, (c) T3, (d) T4, (e) T5, (f) T6, (g) T7, and (h) T8.

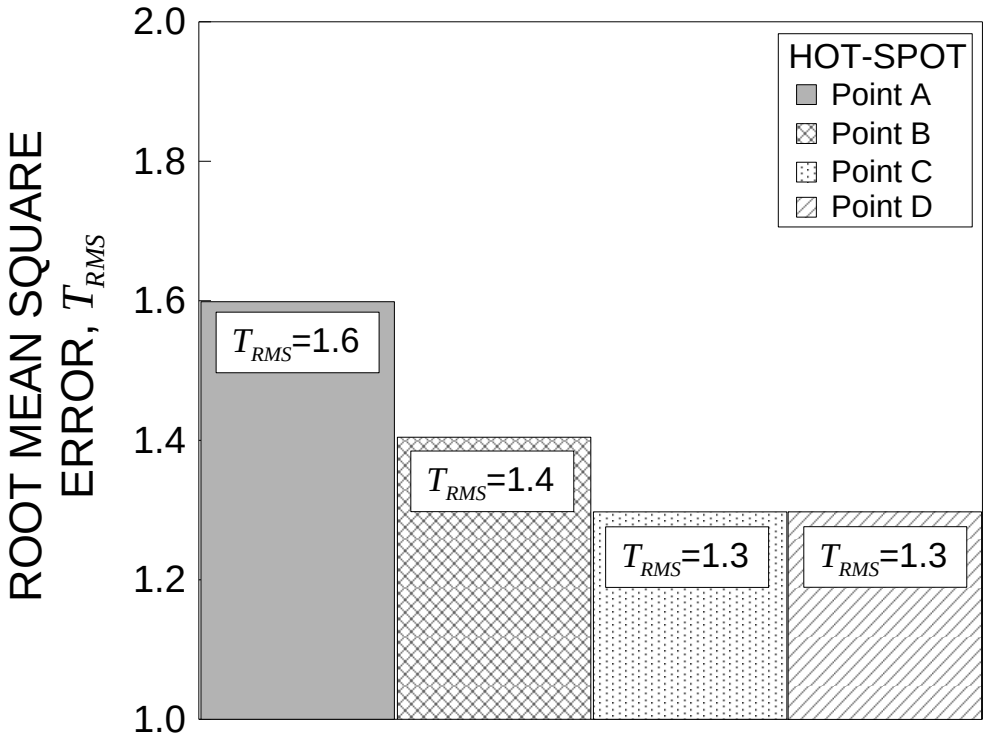

Figure 6. T_{RMS} value for the evaluations performed by considering different hot-spot locations.

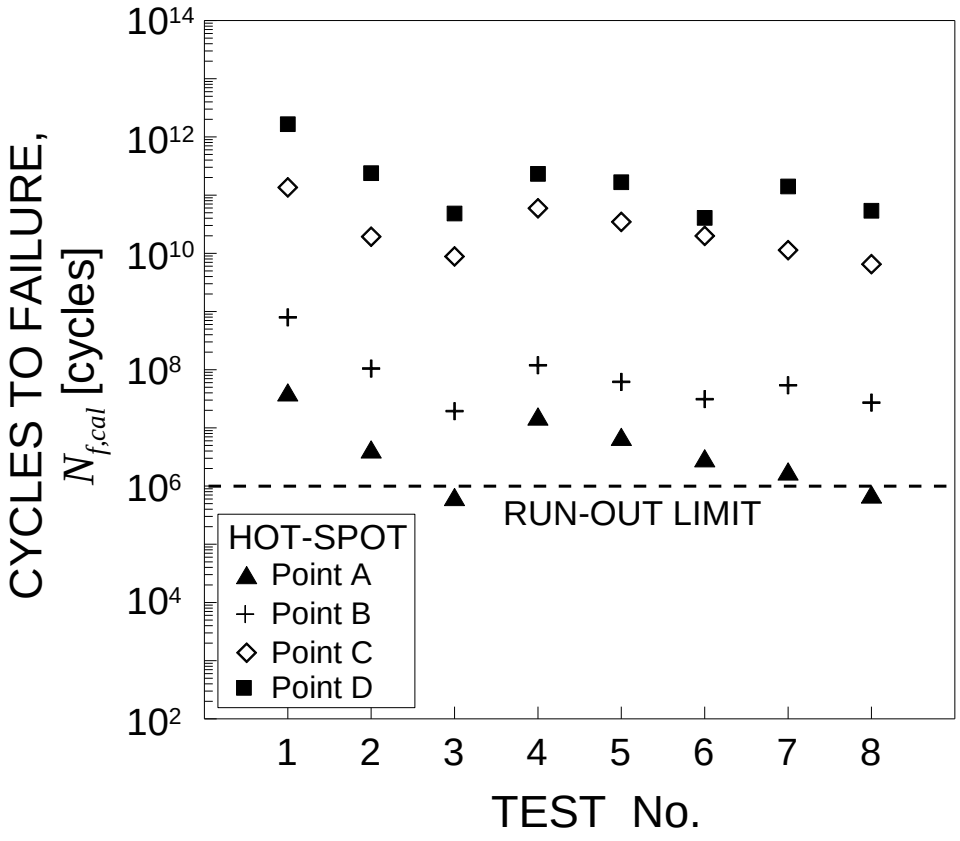

Figure 7. Number of loading cycles to failure evaluated by employing point A, B, C, or D as the hot-spot for each test examined.

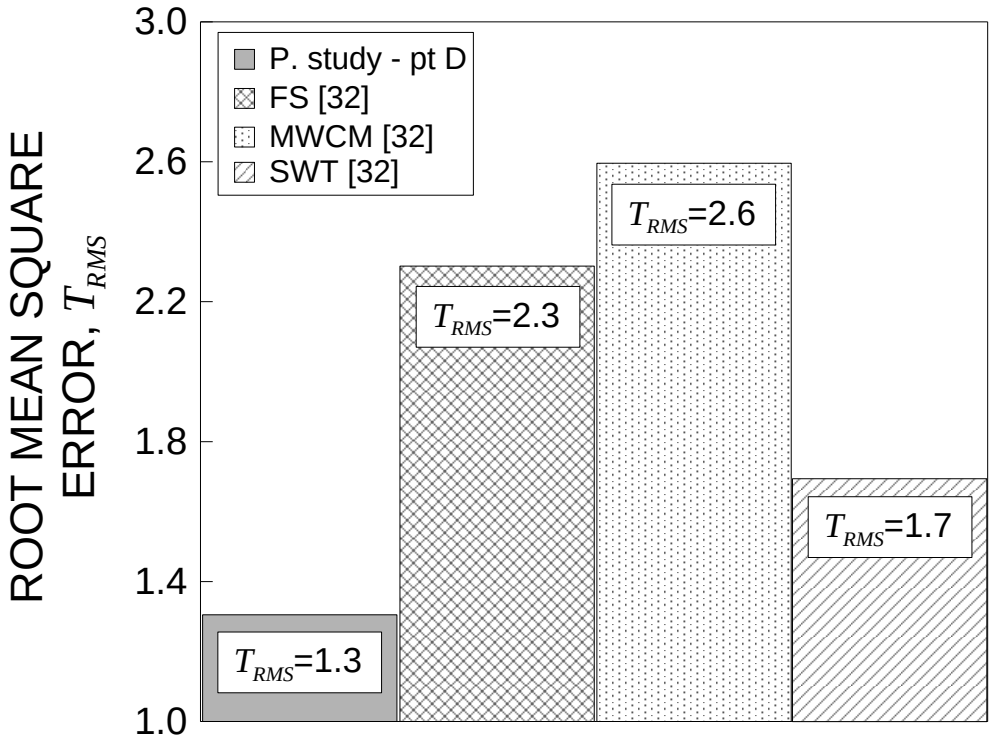

Figure 8. Comparison in terms of T_{RMS} between the present results for hot-spot assumed at point D, and the theoretical results available in the literature **[32].**